Chinese Chemical Letters 35 (2024) 109777

Contents lists available at ScienceDirect

Chinese Chemical Letters

journal homepage: www.elsevier.com/locate/cclet

Surface doping effect on the optoelectronic performance of 2D organic crystals based on cyano-substituted perylene diimides

Jaeyong Ahn[a,1], Zhenping Li[b,1], Zhiwei Wang[b], Ke Gao[b], Huagui Zhuo[b], Wanuk Choi[c], Gang Chang[d], Xiaobo Shang[b,*], Joon Hak Oh[a,*]

[a] School of Chemical and Biological Engineering, Institute of Chemical Processes, Seoul National University, Seoul 08826, South Korea
[b] State Key Laboratory for Mechanical Behavior of Materials, Shaanxi International Research Center for Soft Matter, School of Materials Science and Engineering, Xi'an Jiaotong University, Xi'an 710049, China
[c] Center for Ordered Nanoporous Materials Synthesis, School of Environmental Science and Engineering, Pohang University of Science and Technology, Gyeongbuk 37673, South Korea
[d] Instrumental Analysis Center of Xi'an Jiaotong University, Xi'an 710049, China

ARTICLE INFO

Article history:
Received 11 January 2024
Revised 12 March 2024
Accepted 14 March 2024
Available online 16 March 2024

Keywords:
Doping effect
Phototransistors
Perylene diimides
Organic crystals
Cyano substitution

ABSTRACT

Compared to organic thin films, organic single crystals offer significant potential in organic phototransistors (OPTs) due to their enhanced charge transport, large surface area, and defect-free nature. However, the development of n-type semiconductors has lagged behind p-type semiconductors. To enhance semiconductor device performance, a doping process can be employed, which typically involves the introduction of charged impurities into the crystalline semiconducting material. Its aim is to reduce the Ohmic losses, increase carrier density, improve transport capabilities, and facilitate effective carrier injection, ultimately enhancing the electrical properties of the material. Traditional doping processes, however, often pose a risk of damaging the structure of single crystals. In this study, we have synthesized novel cyano-substituted chiral perylene diimides, which self-assemble into two-dimensional single crystals that can be used for n-type semiconductor devices. We have employed a surface doping strategy using diethylamine vapor without disrupting the crystal structure. The fabricated devices exhibit significantly higher charge transport properties after doping, achieving a maximum electron mobility of 0.14 $cm^2 V^{-1} s^{-1}$, representing an improvement of over threefold. Furthermore, the optoelectronic performance of the doped devices has significantly improved, with the external quantum efficiency increased by over 9 times and the significantly improved response time. These results suggest that our surface doping technology is a promising way for enhancing the performance of 2D organic single-crystal OPTs.

Organic field-effect transistors (OFETs) have attracted a great deal of attention and have been widely used in large-area, flexible and printable electronics due to their simple fabrication, low-cost, strong adjustability, and light weight [1,2]. In particular, organic phototransistors (OPTs) have the ability to tune the density of the charge carriers under incident light stimuli because of the third electrode [3]. Among the various types of OPTs, organic small molecule single crystals are promising candidates for application in OPTs owing to their large surface area, and defect-free nature with long exciton diffusion length and high charge carrier mobility [4–6]. Two-dimensional (2D) organic crystals combine the inherent advantages of organic photoactive layers with the characteristics of 2D structures. Their unique 2D planar morphology, low manufacturing cost, and lightweight nature make them highly valuable for high-performance organic electronics, offering photoresponsive functions, enhanced charge transport, and facile device fabrication [7–9]. Although n-channel materials are required for implementing complementary logic circuits, the development of n-type materials and their optoelectronic performances in OPTs still lag behind p-type counterparts [10,11].

Doping refers to introducing impurities into the intrinsic semiconductors to modulate their electrical, optical, and structural properties [5]. It is a promising technology, which can improve carrier density, transport capacity, and effective carrier injection by reducing the Ohmic loss [12]. Doping in intrinsic semiconductors can be categorized into n-type doping and p-type doping based on whether the majority carriers, after doping, are electrons or

* Corresponding authors.
E-mail addresses: xiaoboshang@xjtu.edu.cn (X. Shang), joonhoh@snu.ac.kr (J.H. Oh).
[1] These authors contributed equally to this work.

https://doi.org/10.1016/j.cclet.2024.109777
1001-8417/

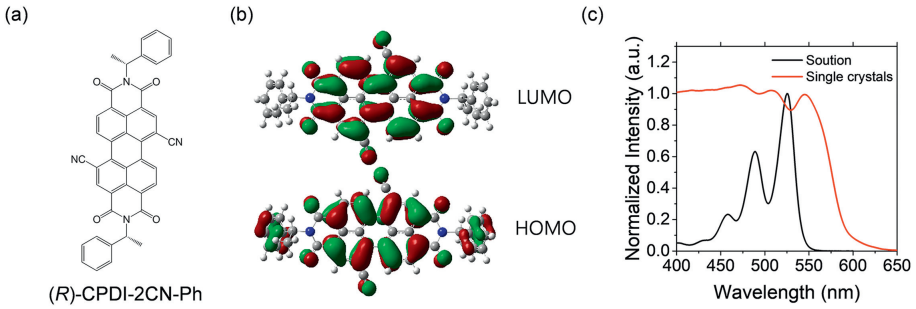

Fig. 1. (a) Chemical structure of (*R*)-CPDI-2CN-Ph. (b) Charge-density isosurfaces of the LUMO and HOMO of (*R*)-CPDI-2CN-Ph monomer estimated from the DFT calculation. (c) UV–vis spectra of (*R*)-CPDI-2CN-Ph in chloroform solution (10^{-4} mol/L) and its self-assembled single crystals deposited on a quartz plate.

holes. The demand for high-performance n-doped semiconductors is increasing for achieving complementary circuits with low power consumption and operational stability. However, they are still rarer than p-doped semiconductors [13]. With the rapid development of organic light-emitting diodes (OLEDs) [14], organic solar cells [15], and OFETs [16,17], n-doped semiconductors become increasingly important in improving device efficiency and enhancing device stability [18–20].

To achieve an efficient electron transfer, the ionization energy of n-dopant needs to be lower than the lowest unoccupied molecular orbital (LUMO) energy of organic semiconductors (OSCs) [12]. To avoid using air-sensitive materials directly, the precursors, which can release reducing n-dopants *in situ* during the processing, have been widely used in organic electronics, such as inorganic salts, organic salts, organic hydrides, and dimers [12]. Other new categories of n-dopants besides reducing species and their precursors have also been reported, including anions and amidine derivatives [12,21,22]. Among various doping methods including coprocessing and sequential doping, surface vapor doping is more attractive because it is less detrimental to OSCs. Amines with strong electron donating nature are good candidates for surface doping.

Perylene diimides (PDIs) with large π-conjugation system are regarded as one of the most promising n-type semiconductors owing to their accessibility, chemical stability, high electron affinity, and their optical/electronic properties [23–26]. Chiral OSCs have recently emerged as highly promising candidates for next-generation optoelectronics [27–29]. However, research on chiral semiconducting PDIs is quite rare, and their performances in OPTs are still not high. In comparison with PDIs with *N*-substituted groups at the imide position, bay-substitution on PDIs can be used to tune optoelectronic properties and solubility of PDIs [30]. Dicyanated PDIs (PDI-2CN) have received significant attention due to their unique combination of high electron mobility, environmental electron stability, solution-processability, and self-assembling properties into micro/nano materials [31–36]. They have been widely used in OFETs by adopting thermal-evaporated or solution-processed thin films and single crystals. Chiral PDI-2CN thin film formed by blending with an insulating polymer has been applied in OPTs [24]. However, there have been few studies conducted on chiral PDI-2CN single crystals for optoelectronics.

Herein, we describe the synthesis and self-assembly process of a chiral PDI-2CN named (*R*)-CPDI-2CN-Ph into 2D materials. Their crystal structures and optoelectronic properties were investigated using X-ray diffraction (XRD) analysis and device measurements, respectively. The average electron mobility of pristine (*R*)-CPDI-2CN-Ph single crystal-based OPTs was 0.011 $cm^2\ V^{-1}\ s^{-1}$. After surface doping process with diethylamine, this mobility increased to 0.036 $cm^2\ V^{-1}\ s^{-1}$. Furthermore, these OPTs exhibited enhanced photodetection properties, with an external quantum efficiency (EQE) and specific detectivity (D^*) value of up to 6342% and 4.6×10^{11} Jones, respectively, accompanied by a faster response time of around 60 milliseconds (ms). These results demonstrate a simple yet effective method for enhancing the performance of organic optoelectronic devices.

(*R*)-CPDI-2CN-Ph was synthesized from di–bromo PTCDA with (*R*)-1-phenylethylamine and the subsequent cyanization. The details are described in Supporting information. Solution of (*R*)-CPDI-2Br-Ph (500 mg, 0.7 mmol) and CuCN (0.9 g, 10 mmol) in DMF (50 mL) was heated to reflux under nitrogen for 24 h. After concentration, the residue was purified by chromatography on silica gel (CH_2Cl_2) and recrystallized (CH_2Cl_2/MeOH) to give (*R*)-CPDI-2CN-Ph (Fig. 1a). Based on the cyclic voltammetry (CV) analysis (Fig. S1 in Supporting information) and density functional theory (DFT) calculation (Fig. 1b), (*R*)-CPDI-2CN-Ph exhibited a similar energy band gap to that of typical bay-substituted PDI materials [30]. However, the high electron affinity of the cyano group in (*R*)-CPDI-2CN-Ph resulted in deep-lying LUMO level. This was evidenced by a LUMO level of −4.16 eV in DFT calculation and −4.21 eV in CV analysis, as shown in Table S1 (Supporting information). (*R*)-CPDI-2CN-Ph single crystals were fabricated through recrystallization method using difference in solubility between toluene and methanol. Methanol vapor slowly diffused into a 1 mg/mL toluene solution in a sealed vial over 3−4 days, resulting in the formation of self-assembled single crystals. As illustrated in Fig. 1c, (*R*)-CPDI-2CN-Ph dissolved in chloroform exhibited clear absorbance spectra in the visible wavelength region. It displayed four main peaks at 525, 489, 458, and 434 nm, corresponding to 0–0, 0–1, 0–2, and 0–3 vibronic transitions of the individual molecules, respectively. On the other hand, the absorbance of fabricated single crystals was red-shifted by around 20 nm compared to the solution, arising from the strong intermolecular interactions. Circular dichroism (CD) measurements exhibited amplified supramolecular chirality in the fabricated single crystals, while (*R*)-CPDI-2CN-Ph in chloroform solution (1.0×10^{-4} mol/L) did not exhibit CD signals in the visible wavelength region. This suggests a chirality transfer from its chiral pendants to the PDI core (Fig. S2 in Supporting information).

The morphological characteristics of (*R*)-CPDI-2CN-Ph single crystals were investigated using scanning electron microscopy (SEM). As shown in Fig. 2a and Fig. S3 (Supporting information), the size of the formed crystals ranged between 20 and 200 μm, with 2-dimensional tetragonal shape. The crystal structure of (*R*)-CPDI-2CN-Ph was studied using single-crystal X-ray diffraction (XRD) analysis to gain a better understanding of its molecular arrangement (Figs. 2b and c). This analysis revealed that (*R*)-CPDI-2CN-Ph crystalized in the triclinic *P*1 space group, and this molecule has a planar PDI core structure, in contrast to halogen-substituted bay structures, which exhibit twisted backbone structures [9,30,37]. The planar PDI core further forms a 2D sheet through the CH···N hydrogen bonding between the diagonal direction of the conjugated plane, while exhibiting slipped stacking with adjacent layers (Fig. 2d). The intermolecular shortest distance between aromatized carbon atoms was 3.45 Å, which is consis-

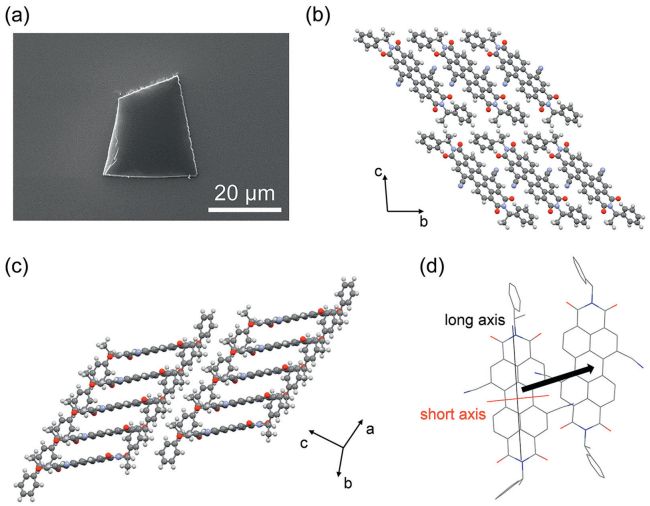

Fig. 2. (a) A SEM image of (*R*)-CPDI-2CN-Ph organic single crystal formed by diffusion of methanol into the toluene solution. Crystal structure of (*R*)-2CN-CDPI-Ph, (b) *a*-axis projection, and (c) drawing of π–π stacking for the (*R*)-CPDI-2CN-Ph. (d) Stacked layers of (*R*)-2CN-CDPI-Ph shifted by half their short length, forming a layered 2D sheet structure. Color code: C, gray; N, light blue; O, red; H, white.

tent with other reported PDIs (Fig. S4 in Supporting information) [38].

To investigate the optoelectronic properties of (*R*)-CPDI-2CN-Ph single crystals, OPTs with bottom-gate top-contact configuration were fabricated. The single crystals dispersed in ethanol were drop-cast on the *n*-octadecyltrimethoxysilane (OTS) treated SiO_2/Si wafers followed by thermal annealing at 60 °C overnight to remove the residual solvent. Then, 150 nm of gold source and drain electrodes were thermally evaporated under a high vacuum condition ($<5 \times 10^{-6}$ torr). The optical microscope images of the fabricated OPT devices are illustrated in Fig. S5 (Supporting information). Charge transport characteristics of individual single crystals were investigated using the fabricated OPTs under dark and vacuum condition ($<10^{-2}$ torr). Amine surface doping was conducted using diethylamine as an n-type dopant to enhance the optoelectronic performance of (*R*)-CPDI-2CN-Ph single crystals based OPTs. The OPT devices were exposed to saturated diethylamine vapor for 30 min at 50 °C under a nitrogen-filled closed space as illustrated in Fig. 3a. For the comparison, both pristine and doped OPTs were measured respectively. The pristine OPTs exhibited typical n-type characteristics with an average electron mobility of 0.011 cm^2 V^{-1} s^{-1}, an on/off ratio ($I_{on/off}$) over 10^3, and a threshold voltage (V_T) of around 1.8 V (Fig. 3b).

After doping, there were clear enhancements in the electrical properties as shown in Fig. 3c. The average electron mobility increased approximately over 3 times and reached 0.036 cm^2 V^{-1} s^{-1} and the threshold voltage negatively shifted to −17.0 V, while maintaining the on/off ratio value over 10^3. The maximum electron mobility could reach 0.14 cm^2 V^{-1} s^{-1}, which is significantly higher than the undoped samples. This strong *n*-doping effect was also confirmed from the output curves of the pristine and doped devices (Fig. 3d). The enhanced mobilities suggest that diethylamine efficiently transferred electrons to the (*R*)-CPDI-2CN-Ph single crystals. In the electron spin resonance (ESR) spectral analysis, a strong signal enhancement with a *g*-factor of 2.0051 was observed after doping with diethylamine (Fig. 3e). This result indicates the formation of radical anions, which can contribute to π-electron delocalization. This enables charge carrier transport through the intermolecular π-π stacking, thereby enhancing charge carrier mobility [9,21]. Minor peaks observed in pristine crystals might result from structural defects or traps. The effective doping process also resulted from the elimination of electron traps at the step edges of crystals, which are detrimental for charge transport [39]. This is further substantiated by the calculated number of deep interface trap states (N_{trap}) from the subthreshold regime (Eq. 1) [40],

$$N_{trap} = C_i|V_T - V_{on}|/e \quad (1)$$

where C_i is the gate dielectric capacitance, V_{on} is the onset voltage, and e is the elementary charge. As shown in Table S2 (Supporting information), the doped (*R*)-CPDI-2CN-Ph single crystals demonstrated a reduced N_{trap} compared with the pristine condition. In addition, absorption spectra also exhibited mild doping effects (Fig. 3f). Impressively, our mild doping strategy not only enhanced the electrical performances but also maintained the on/off ratio of OFETs and the operational stability.

The pristine and doped (*R*)-CPDI-2CN-Ph single crystal based OPTs were illuminated with a 520 nm monochromatic light source

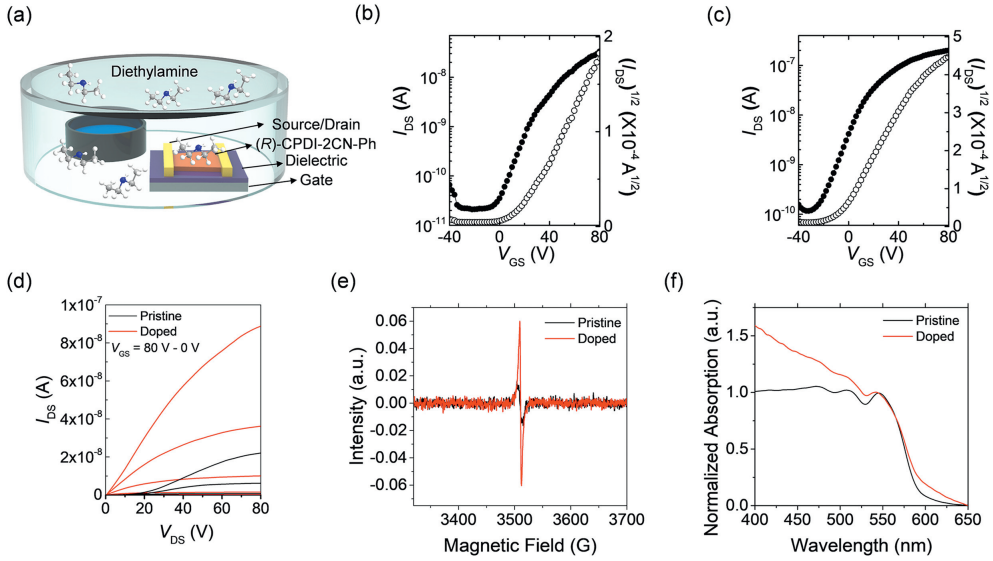

Fig. 3. (a) Schematic illustrations of fabricated OPT device and its doping process. Transfer characteristics of (b) pristine and (c) doped (*R*)-CPDI-2CN-Ph single crystal based OPTs. (d) Output characteristics of pristine and doped (*R*)-CPDI-2CN-Ph single crystal based OPTs. (e) ESR spectra of pristine and doped (*R*)-CPDI-2CN-Ph single crystals. (f) UV–vis spectra of pristine and doped (*R*)-CPDI-2CN-Ph single crystals.

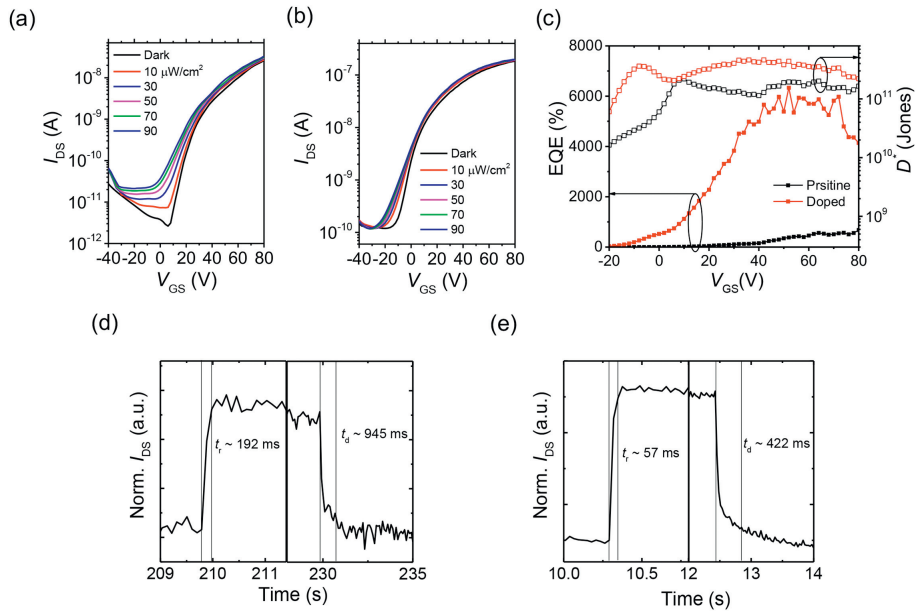

Fig. 4. Transfer characteristics of (*R*)-CPDI-2CN-Ph single crystal based OPTs (a) before and (b) after diethylamine doping under monochromatic light irradiation varying in intensity ($\lambda = 520$ nm). (c) EQE and D^* results of pristine and doped (*R*)-CPDI-2CN-Ph single crystal based OPTs. Photoresponse time of (d) pristine and (e) doped (*R*)-CPDI-2CN-Ph single crystal based OPTs. All measurements were taken under vacuum conditions.

to further investigate the optoelectronic properties. Both devices exhibited photodoping phenomena of an increased source-drain current (I_{DS}) and a negatively shifted V_T under light illumination (Figs. 4a and b). When the light intensity increased from 10 μW/cm^2 to 90 μW/cm^2, a gradual increase of I_{DS} and a negative shift of V_T were observed, due to the trapping of photogenerated charge carriers. Since the trap sites were eliminated from the diethylamine doping process, the degree of V_T shift was much clear in the pristine devices. Several figures of merit, such as EQE, and D^*, were calculated to compare the photodetection properties of (*R*)-CPDI-2CN-Ph single crystal based OPTs before and after diethylamine doping, based on the transfer curves (Fig. 4c and Table S3 in Supporting information). The pristine OPTs exhibited the maximum EQE, and D^* values of 674%, and 2.2×10^{11} Jones respectively, under 90 μW/cm^2 monochromatic light irradiation. After 30 min of diethylamine doping, they exhibited greatly improved optoelectronic performances while reaching the maximum EQE, and D^* values of 6342%, and 4.6×10^{11} Jones, respectively. These improved values originated from the enhanced charge carrier mobilities, which facilitated the efficiency of exciton separation, thereby contributing to the enhancement of photocurrent. Since the doping process not only increased the photocurrent but also increased the dark current of the devices by electron transfer, the degree of enhancement of D^* values (over 2 times) was lower than the EQE values (over 9 times).

The photoresponse time of pristine and doped OPTs was also measured upon monochromatic light irradiation. The rise and decay times were extracted from the time required for the current to rise to 90% and decay to 10% of the peak value under light illumination. The pristine single crystal based OPTs detected the visible light (520 nm) within the millisecond scale (rise time for 192 ms and decay time for 945 ms) as shown in Fig. 4d. On the other hand, the doped devices could respond to the light more rapidly, with the switching speeds within 57 ms and 422 ms for rise and decay time, respectively (Fig. 4e). After doping, the number of traps was reduced and charge carrier mobility was enhanced, which resulted in faster trap filling and release. Our doping strategy suggests an efficient way to improve not only the sensitivity of single crystal based OPTs, but also photoresponse time using a simple and non-destructive method. Therefore, this study paves the way for practical photodetector applications using organic semiconductor single crystals.

In conclusion, a novel chiral cyano-substituted PDI material was synthesized and self-assembled into 2D single crystals. Crystal structure analysis revealed that the 2D sheet was formed by the slipped stacking induced by the CH···N hydrogen bonding. OPTs with a bottom-gate top-contact configuration were fabricated to investigate the photoelectric properties of (*R*)-CPDI-2CN-Ph single crystals. To enhance the performance of OPTs, (*R*)-CPDI-2CN-Ph single crystals were exposed to saturated diethylamine vapor for the non-destructive surface doping. This led to an increase in the average electron mobility by over threefold, reaching 0.036 cm^2 V^{-1} s^{-1}, with the maximum electron mobility of 0.14 cm^2 V^{-1} s^{-1}. This suggests that diethylamine effectively transferred electrons to (*R*)-CPDI-2CN-Ph single crystals. The formation of radical anions contributed to π-electron delocalization, facilitating carrier mobility improvement through intermolecular π-π stacking transport. Furthermore, the calculated N_{trap} confirms that effective doping processes eliminate electron traps that are unfavorable for charge transport at the crystal edges. After doping, EQE and D^* of OPTs effectively increased to 6342% (~9 times) and 4.6×10^{11} Jones (~2 times), respectively, with the faster response time due to the enhanced charge transport characteristics and reduced number of traps. Our research findings demonstrate that doping can greatly improve the photodetection performance of OPTs, paving an effective way for the widespread application of organic photodetectors.

Declaration of competing interest

The authors declare that they have no known competing financial interests or personal relationships that could have appeared to influence the work reported in this paper.

Acknowledgments

This work was supported by the National Research Foundation (NRF) of Korea (Nos. 2023R1A2C3007715, 2021R1A4A1032515, RS-2023-00281944) and funded by the Ministry of Science and ICT

(MSIT) of Korea. This work was also supported by Korea Toray Science Foundation, Shaanxi Fundamental Science Research Project for Chemistry & Biology (No. 22JHQ035) and Natural Science Basic Research Program of Shaanxi Province (No. 2024JC-YBMS-081). The Institute of Engineering Research at Seoul National University provided research facilities for this work.

Supplementary materials

Supplementary material associated with this article can be found, in the online version, at doi:10.1016/j.cclet.2024.109777.

References

[1] H.T. Yi, M.M. Payne, J.E. Anthony, et al., Nat. Commun. 3 (2012) 1259.
[2] M.Y. Lee, H.R. Lee, C.H. Park, et al., Acc. Chem. Res. 51 (2018) 2829–2838.
[3] K.J. Baeg, M. Binda, D. Natali, et al., Adv. Mater. 25 (2013) 4267–4295.
[4] T. Hasegawa, J. Takeya, Sci. Technol. Adv. Mater. 10 (2009) 024314.
[5] I. Song, X. Shang, J. Ahn, et al., Chem. Mater. 34 (2022) 8675–8683.
[6] C. Zhao, M.U. Ali, J. Ning, et al., Front. Phys. 16 (2021) 43202.
[7] S.K. Park, J.H. Kim, S.Y. Park, Adv. Mater. 30 (2018) 1704759.
[8] F. Yang, S. Cheng, X. Zhang, et al., Adv. Mater. 30 (2018) 1702415.
[9] X. Shang, I. Song, J.H. Lee, et al., ACS Nano 14 (2020) 14146–14156.
[10] U. Kraft, M. Sejfić, M.J. Kang, et al., Adv. Mater. 27 (2015) 207–214.
[11] B. Mukherjee, Optik 139 (2017) 48–55.
[12] Z. Bin, Z. Liu, Y. Qiu, et al., Adv. Opt. Mater. 6 (2018) 1800536.
[13] D. Yuan, W. Liu, X. Zhu, Chem. Soc. Rev. 52 (2023) 3842–3872.
[14] K.H. Kim, J.L. Liao, S.W. Lee, et al., Adv. Mater. 28 (2016) 2526–2532.
[15] Y. Lin, M.I. Nugraha, Y. Firdaus, et al., ACS Energy Lett. 5 (2020) 3663–3671.
[16] L. Jiang, H. Dong, W. Hu, J. Mater. Chem. 20 (2010) 4994.
[17] L. Cao, C. Ren, T. Wu, J. Mater. Chem. C 11 (2023) 3428–3447.
[18] J.H. Oh, S.L. Suraru, W.Y. Lee, et al., Adv. Funct. Mater. 20 (2010) 2148–2156.
[19] J.H. Oh, P. Wei, Z. Bao, Appl. Phys. Lett. 97 (2010) 243305.
[20] P. Wei, J.H. Oh, G. Dong, et al., J. Am. Chem. Soc. 132 (2010) 8852–8853.
[21] H. Wei, P.A. Chen, J. Guo, et al., Adv. Funct. Mater. 31 (2021) 2102768.
[22] H. Wei, Z. Cheng, T. Wu, et al., Adv. Mater. 35 (2023) 2300084.
[23] X. Shang, I. Song, H. Ohtsu, et al., Adv. Mater. 29 (2017) 1605828.
[24] I. Song, J. Ahn, X. Shang, et al., ACS Appl. Mater. Interfaces 12 (2020) 49926–49934.
[25] C. Huang, S. Barlow, S.R. Marder, J. Org. Chem. 76 (2011) 2386–2407.
[26] X. Shang, I. Song, H. Ohtsu, et al., Sci. Rep. 7 (2017) 5508.
[27] I. Song, J. Ahn, H. Ahn, et al., Nature 617 (2023) 92–99.
[28] J. Ahn, S.H. Lee, I. Song, et al., Device 1 (2023) 100176.
[29] L. Zhang, I. Song, J. Ahn, et al., Nat. Commun. 12 (2021) 142.
[30] X. Shang, J. Ahn, J.H. Lee, et al., ACS Appl. Mater. Interfaces 13 (2021) 12278–12285.
[31] J.H. Oh, Y.S. Sun, R. Schmidt, et al., Chem. Mater. 21 (2009) 5508–5518.
[32] R.T. Weitz, K. Amsharov, U. Zschieschang, et al., J. Am. Chem. Soc. 130 (2008) 4637–4645.
[33] F. Liscio, S. Milita, C. Albonetti, et al., Adv. Funct. Mater. 22 (2012) 943–953.
[34] I. Vladimirov, M. Kellermeier, T. Geßner, et al., Nano Lett. 18 (2018) 9–14.
[35] B.A. Jones, M.J. Ahrens, M.H. Yoon, et al., Angew. Chem. Int. Ed. 43 (2004) 6363–6366.
[36] A.S. Molinari, H. Alves, Z. Chen, et al., J. Am. Chem. Soc. 131 (2009) 2462–2463.
[37] M. Gsänger, J.H. Oh, M. Könemann, et al., Angew. Chem. Int. Ed. 49 (2010) 740–743.
[38] P. Zugenmaier, J. Duff, T.L. Bluhm, Cryst. Res. Technol. 35 (2000) 1095–1115.
[39] T. He, M. Stolte, Y. Wang, et al., Nat. Mater. 20 (2021) 1532–1538.
[40] N. Shin, J. Zessin, M.H. Lee, et al., Adv. Funct. Mater. 28 (2018) 1802265.